Fully quantum calculations of O2-N2 scattering using a new potential energy surface: Collisional perturbations of the oxygen 118 GHz fine structure line

M. Gancewski, H. Jóźwiak, E. Quintas-Sánchez, R. Dawes, Franck Thibault, P. Wcislo

Fully quantum calculations of O_2–N_2 scattering using a new potential energy surface: Collisional perturbations of the oxygen 118 GHz fine structure line

Maciej Gancewski,[1, a)] Hubert Jóźwiak,[1] Ernesto Quintas-Sánchez,[2] Richard Dawes,[2] Franck Thibault,[3] and Piotr Wcisło[1, b)]

[1)] *Institute of Physics, Nicolaus Copernicus University in Toruń, Grudziadzka 5, 87-100 Toruń, Poland*

[2)] *Department of Chemistry, Missouri University of Science and Technology, Rolla, MO 65409-0010, USA*

[3)] *Univ. Rennes, CNRS, IPR (Institut de Physique de Rennes)-UMR 6251, Rennes F-35000, France*

(Dated: 5 October 2021)

A proper description of the collisional perturbation of the shapes of molecular resonances is important for remote spectroscopic studies of the terrestrial atmosphere. Of particular relevance are the collisions between the O_2 and N_2 molecules – the two most abundant atmospheric species. In this work, we report a new highly accurate $O_2(X^3\Sigma_g^-)$–$N_2(X^1\Sigma_g^+)$ potential energy surface and use it for performing the first quantum-scattering calculations addressing line shapes for this system. We use it to model the shape of the 118 GHz fine structure line in O_2 perturbed by collisions with N_2 molecules, a benchmark system for testing our methodology in the case of an active molecule in a spin triplet state. The calculated collisional broadening of the line agrees well with the available experimental data over a wide temperature range relevant for the terrestrial atmosphere. This work constitutes a step towards populating the spectroscopic databases with *ab initio* line-shape parameters for atmospherically relevant systems.

I. INTRODUCTION

Molecular nitrogen is the most abundant constituent of the terrestrial atmosphere. Collisions involving N_2 impact the properties of other atmospheric species in a significant way. Such perturbations must be accounted for in studies of Earth's atmosphere which rely heavily on spectroscopic methods. Accurate knowledge of the collision-perturbed shapes of spectral lines is crucial to interpret remote sensing spectroscopic data, and reliable modelling of the terrestrial properties (such as Earth's carbon cycle[1], polutant gas concentrations[2,3] and temperature profiling[4]) depends on the extent to which such effects are employed in a given line-shape model.

Among the molecular species of atmospheric importance affected by presence of the N_2 bath, O_2 is of special interest. It is the second most abundant terrestrial molecule, and it plays a major role in many land- and satellite-based remote sensing applications.[5–9] It is also a prominent example of a diatomic species with a $^3\Sigma$ ground electronic state, which makes it a perfect candidate for studying the fine-structure-resolved molecular transitions in the context of atmospheric science. The oxygen spectral bands formed by transitions to excited electronic states, such as the *A*- and *B*-band, are studied extensively due to their application in the determination of cloud-top heights and coverage,[10] optical thickness of aerosols,[6] concentration of the polutant CO_2,[2,3] temperature profiling,[4] recovering surface pressure,[11] monitoring of the greenhouse gases[1,7] and vegetation fluorescence.[12]

Many such applications also involve transitions occurring within the ground electronic and vibrational $^3\Sigma_g^-(\nu = 0)$ state of O_2. The symmetries associated with its electronic term result in the existence of only odd rotational levels, which are split into a triplet of fine structure states by the spin–spin interactions of two unpaired electrons.[13,14] The possible transitions are denoted N_a+ and N_a- (where N_a is the rotational quantum number of oxygen), which corresponds to transitions satisfying the selection rules for the total angular momentum j, respectively, $j = N_a \to j = N_a + 1$ and $j = N_a \to j = N_a - 1$.[15,16] Oxygen has a strong spectral band between 50 and 70 GHz (known as the 60 GHz band) and a single isolated line at approximately 118 GHz, which corresponds to the $1-$ transition.[17,18] These spectral features arise from purely fine structure transitions within rotational levels of O_2. The 60 GHz oxygen band and 118 GHz line perturbed by N_2 have been studied extensively due to their applications in remote sensing observations and temperature profiling.[15–22]

In this paper, we report a new *ab initio* potential energy surface (PES) for the $O_2(X^3\Sigma_g^-)$–$N_2(X^1\Sigma_g^+)$ system, and we use it in quantum scattering calculations of the shape of the N_2-perturbed 118 GHz fine structure $1-$ line in O_2. Since the O_2–N_2 interaction is of electrostatic origin and depends very weakly on electron spin, we make use of the powerful recoupling techniques of Corey and McCourt,[23] and Alison Offer *et al.*[24] to reduce the problem of $^3\Sigma$ diatom–$^1\Sigma$ diatom scattering to collisions involving two $^1\Sigma$ rigid rotors. We determine the broadening coefficient of the 118 GHz line in O_2 due to collisions with N_2 by changing the total angular momentum representation of the S-matrix obtained from the spin-free quantum scattering calculations. These calculations are

[a)] Corresponding author (E-mail): mgancewski@op.pl

[b)] E-mail: piotr.wcislo@umk.pl

performed using the exact close-coupling approach.[25]

The oxygen 118 GHz line is special in the sense that the corresponding transitions occur between molecular states for which the effective Hamiltonian of O_2 is diagonal,[26,27] hence, in our approach, there is no need to introduce the fully coupled representation of the oxygen Hamiltonian for the sake of scattering calculations. Our *ab initio* results agree with the available experimental data.[15,16,20,21,28] The O_2–N_2 collisional system plays a benchmark role for studying the transitions occurring within single rotational levels of atmospheric molecules, the results of such studies being important for accurate modelling and calculations of *ab initio* line parameters for systems of atmospheric interest in Earth as well as exoplanetary studies, and populating the spectroscopic databases with high-accuracy theoretical results. So far, in this context, extensive *ab initio* quantum-scattering calculations of the line-shape parameters were performed for the simple systems of He-perturbed H_2[29–33] and HD[34,35], which are relevant for the atmospheres of Solar System gas giants and some types of exoplanets. Recently, these results were used to generate comprehensive beyond-Voigt line-shape parameter dataset for these two systems[36,37] that are consistent with the HITRAN double-power-law representation.[38] Similar work is in progress for N_2-perturbed CO, which is relevant for Earth's atmosphere; recently the first results were published in Ref. 39. This work is in line with those developments, but addresses more challenging systems for which the active molecule is in the triplet spin state.

This paper is organized as follows. In Section II, we briefly review the theory of scattering between two $^1\Sigma$ rigid rotors and discuss its generalization to the case in which one of the collision partners is in the $^3\Sigma$ state with a non-vanishing electron spin. We discuss the form of the effective Hamiltonian of the $O_2(^3\Sigma_g^-)$ monomer and the transformation between the electronic spin-free and the total angular momentum representations of the scattering S-matrix. In Section III, we describe the methodology used to determine the O_2–N_2 PES, its topography and basic characteristics, and we provide the decomposition of the PES into its angular and radial parts, the latter being used in the scattering calculations. We discuss the computational details of our close-coupling simulations of O_2–N_2 collisions in Sec. IV, and we also analyze there the pressure broadening cross sections obtained from the quantum scattering calculations. In Section V, we discuss our calculations of the collisional broadening parameters for the N_2-perturbed 118 GHz fine structure line in O_2 and we compare our results with experimental data. Finally, we summarize our results and put them in perspective with future work in Sec. VI.

II. THEORY

One may formulate the dynamics of molecule–molecule collisions by solving the time-independent Schrödinger equation, with the Hamiltonian (given in atomic units)[25]

$$H = -\frac{1}{2\mu R}\frac{\partial^2}{\partial R^2}R + \frac{\boldsymbol{l}^2}{2\mu R^2} + V(R,\vartheta_a,\vartheta_b,\phi) + \mathcal{H}^{(a)} + \mathcal{H}^{(b)}, \tag{1}$$

where $\boldsymbol{l}$ is the orbital angular momentum of relative motion of the colliding species (with μ being their reduced mass), $V(R,\vartheta_a,\vartheta_b,\phi)$ is the intermolecular interaction potential written in the Jacobi coordinates (defined in Fig. 1), and $\mathcal{H}^{(a)}$ and $\mathcal{H}^{(b)}$ denote the internal Hamiltonians of the asymptotically separated monomers a and b.

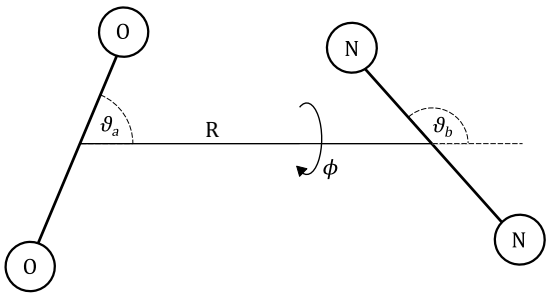

FIG. 1. Definition of the Jacobi coordinates.[40,41] Angles ϑ_i and φ_i (omitted for clarity) give the space-fixed orientation of the i-th monomer, $\phi = \varphi_a - \varphi_b$ is the relative dihedral angle of the two molecules and R is the distance between their mass centers.

In the well-known case of rotationally inelastic scattering between two $^1\Sigma$ rigid rotors,[25,42] $\mathcal{H}^{(a)}$ and $\mathcal{H}^{(b)}$ are the purely rotational Hamiltonians satisfying

$$\left[\mathcal{H}^{(i)} - E_{\mathrm{rot}}^{(i)}\right]|N_i m_i\rangle = 0 \quad , \quad i = a, b, \tag{2}$$

where $E_{\mathrm{rot}}^{(i)}$ is the rotational energy and N_i is the quantum number associated with the nuclei end-over-end rotational angular momentum, with the space-fixed projection m_i. The total angular momentum of the system is then introduced by means of the coupling

$$\mathbf{N} = \mathbf{N}_a + \mathbf{N}_b, \qquad \mathbf{J} = \mathbf{N} + \boldsymbol{l}, \tag{3}$$

with the corresponding eigenbasis given by

$$|(N_a N_b)Nl; JM\rangle = \sum_{m_N, m_l} C^{NlJ}_{m_N m_l M}\,|(N_a N_b)N m_N\rangle \otimes |l m_l\rangle\,, \tag{4}$$

where N is the total rotational quantum number of the colliding pair, l is their relative orbital angular momentum, J is the total angular momentum of the system, m_N, m_l and M are the corresponding space-fixed projection quantum numbers and $C^{j_1 j_2 j_{12}}_{m_1 m_2 m_{12}}$ is the Clebsch-Gordan coefficient.[13,43]

In the absence of external fields, the total angular momentum and its projection are conserved during the collision,[24,43] hence the total wave function Ψ may be labeled

with J and M, and expanded in the total-J basis defined in Eq. (4):

$$\Psi^{JM}_{N_a N_b N l} = \sum_{\substack{N'_a, N'_b, \\ N', l'}} \frac{F^{N'_a N'_b N' l'}_{N_a N_b N l; J}(R)}{R} \, |(N'_a N'_b) N' l'; JM\rangle \,, \tag{5}$$

which allows separating the radial and angular parts of the problem. Substitution of Eq. (5) into the Schrödinger equation yields the usual set of close-coupling equations

$$\Big[\frac{\mathrm{d}^2}{\mathrm{d}R^2} - \frac{l'(l'+1)}{R^2} + k'^2\Big] F^{N'_a N'_b N' l'}_{N_a N_b N l; J}(R) = 2\mu \sum_{\substack{N''_a, N''_b, \\ N'', l''}} V^J_{(N'_a N'_b) N' l', (N''_a N''_b) N'' l''} F^{N''_a N''_b N'' l''}_{N_a N_b N l; J}(R), \tag{6}$$

where $k^2 = 2\mu\big[E - E^{(a)}_{\mathrm{rot}} - E^{(b)}_{\mathrm{rot}}\big]$ is the squared wave vector containing the total collisional energy E. One then solves Eq. (6) numerically with the boundary condition[25]

$$F^{N'_a N'_b N' l'}_{N_a N_b N l; J}(R) \sim \delta_{N_a N'_a} \delta_{N_b N'_b} \delta_{N N'} \delta_{l l'} e^{-i(kR - l\pi/2)} - \sqrt{\frac{k}{k'}} \, \hat{\mathrm{S}}^J_{(N'_a N'_b) N' l', (N_a N_b) N l} \, e^{i(k' R - l'\pi/2)} \tag{7}$$

for large values of the intermolecular distance R, from which the S-matrix elements $\hat{\mathrm{S}}^J_{(N'_a N'_b) N' l', (N_a N_b) N l}$ may be obtained.[44]

The above close-coupling scheme is well known for spin-free molecules in Σ electronic states. However, when the electron and/or nuclear spins are present, this approach must be modified to account for additional scattering channels arising from the coupling between the spin angular momenta and the rotational and orbital motions of the colliding molecules. Indeed, calculations for molecules exhibiting fine[45–59] and hyperfine[60–65] structure have been performed, using both the exact and recoupled close-coupling formalism. The exact approach is based on expanding the total wave function in a basis of eigenfunctions of the monomers' Hamiltonians which, in general, include the terms involving spin interactions. In the recoupled approach these are neglected, and one solves the spin-free problem using the wave function in Eq. (5); the appropriate S-matrix is then expressed as a linear combination of the spin-free S-matrices from the recoupled calculations.

The latter method is especially useful in calculations involving atmospheric molecules, for which the number of coupled channels in Eq. (6) grows considerably with the kinetic energy of the binary collision.[39] In the present case of $\mathrm{O_2}(^3\Sigma^-_g)$–$\mathrm{N_2}(^1\Sigma^+_g)$ scattering, an additional degree of freedom is introduced into the problem by the non-zero electronic spin $\mathbf{S}$ of the ground-state $\mathrm{O_2}$. The fine-structure splitting in $\mathrm{O_2}$ is small compared with the spacings between the rotational levels, hence molecular oxygen may be accurately described within the Hund's case (b) limit.[26] The theoretical framework for treating the scattering between a multiplet–Σ case (b) molecule and a structureless closed-shell atom using the recoupled approach was introduced by Corey and McCourt,[23] and their formulae were generalized by Alison Offer *et al.*[24] to be applicable to hyperfine transitions in bi-molecular collisions. With purely formal modifications this method is also applicable to fine structure transitions in open-shell diatoms. We apply the framework developed in Refs. 23 and 24 to the $\mathrm{O_2}$–$\mathrm{N_2}$ scattering in order to express the S-matrix in the representation that is most convenient for the pressure broadening calculations.

Finally, it should be mentioned that approximating the collision dynamics by the recoupled approach is not always justified,[45,49] and one must then recourse to the exact close-coupling scheme. A notable example is the SO molecule which, just as $\mathrm{O_2}$, has a $^3\Sigma$ ground electronic state. However, in SO($^3\Sigma$) the splitting of fine structure levels is very large, and use of an intermediate coupling between Hund's case (a) and (b) is required rather than the pure case (b) limit (which only becomes attainable in SO for rotational quantum numbers ≥ 5).[48,49] In such cases one cannot ignore the mixing between different rotational states of the open-shell diatomic collision target, and the resulting calculations obviously become much more demanding.[48,49,59,64,65]

Let indices a and b refer to the $\mathrm{O_2}$ and $\mathrm{N_2}$ monomers, respectively. While the rotational $|N_b m_b\rangle$ basis of $\mathrm{N_2}$ is still appropriate to use, the rotational basis for the $\mathrm{O_2}$ monomer is now given by the Hund's case (b) vectors[13,26]

$$|(N_a S) j m\rangle = \sum_{m_a, m_S} C^{N_a S j}_{m_a m_S m} \, |N_a m_a\rangle \otimes |S m_S\rangle \,, \tag{8}$$

where j is the total molecular angular momentum quantum number of $\mathrm{O_2}$ (with projection m), which – unlike N_a – is preserved by electronic spin interactions as a good quantum number.[13,26]

Now, the effective molecular Hamiltonian of the $^3\Sigma^-_g$ state of $\mathrm{O_2}$ may be written as[26,66]

$$\mathcal{H}^{(a)} = \mathcal{H}^{(a)}_{\mathrm{rot}} + \mathcal{H}^{(a)}_{\mathrm{sr}} + \mathcal{H}^{(a)}_{\mathrm{ss}}, \tag{9}$$

where the subsequent terms on the right hand side correspond to the rotational part, the spin–rotation part and the spin–spin interaction part. The ^{16}O nuclei have zero spin, hence for the $^3\Sigma^-_g$ state of molecular oxygen the total wave function is symmetric under permutation of the nuclei.[13,41] Consequently, only the rotational levels for which N_a is odd exist in $\mathrm{O_2}$. The spin–spin interaction splits each rotational level into a triplet of fine structure levels whose energies carry a small contribution from the spin–rotation interaction.[13] In the basis defined by Eq. (8) $\mathcal{H}^{(a)}_{\mathrm{rot}}$ and $\mathcal{H}^{(a)}_{\mathrm{sr}}$ are diagonal, whereas $\mathcal{H}^{(a)}_{\mathrm{ss}}$ mixes states of the same j for which $\Delta N_a = \pm 2$.[26,27] The molecular Hamiltonian matrix has thus a block-diagonal

form:

$$\begin{array}{c} \\ |1,0\rangle \\ |1,1\rangle \\ |1,2\rangle \\ |3,2\rangle \\ \vdots \end{array} \begin{array}{c} \begin{array}{ccccc} |1,0\rangle & |1,1\rangle & |1,2\rangle & |3,2\rangle & \dots \end{array} \\ \begin{pmatrix} \varepsilon_{00}^{(1)} & 0 & 0 & 0 & \dots \\ 0 & \varepsilon_{11}^{(1)} & 0 & 0 & \dots \\ 0 & 0 & \varepsilon_{11}^{(2)} & \varepsilon_{13}^{(2)} & \dots \\ 0 & 0 & \varepsilon_{31}^{(2)} & \varepsilon_{33}^{(2)} & \dots \\ \vdots & \vdots & \vdots & \vdots & \ddots \end{pmatrix} \end{array}, \tag{10}$$

where $|N_a, j\rangle \equiv |(N_a S) jm\rangle$, for brevity, and $\varepsilon_{N'_a N_a}^{(j)}$ are the corresponding matrix elements.

It can be seen that the $\{|1,0\rangle, |1,1\rangle\}$ block is diagonal in the Hund's case (b) basis. Hence one can work solely in this basis when considering the transitions between the $|1,0\rangle$ and $|1,1\rangle$ states only, such as in the case of the 118 GHz fine structure $1-$ line. Since $\mathcal{H}^{(b)} = \mathcal{H}_{\rm rot}^{(b)}$ is diagonal in the rotational basis of the $N_2(^1\Sigma_g^+)$ monomer, to describe the collision dynamics between the two molecules one may couple the angular momenta as[24]

$$\mathbf{j}_R = \mathbf{N}_b + \boldsymbol{l}, \quad \mathbf{j} = \mathbf{N}_a + \mathbf{S}, \quad \mathbf{J}_T = \mathbf{j}_R + \mathbf{j}, \tag{11}$$

where now $\mathbf{J}_T$ is the total angular momentum of the system (excluding nuclear spins) and $\mathbf{j}_R$ is the composite angular momentum associated with the presence of the molecular bath. Consequently, the space-fixed eigenbasis for expanding the total wave function in the Schrödinger equation is defined by

$$|(N_b l) j_R (N_a S) j; J_T M_T\rangle = \sum_{m_R, m} C^{j_R j J_T}_{m_R m M_T} |(N_b l) j_R m_R\rangle \otimes |(N_a S) jm\rangle . \tag{12}$$

However, one may introduce another coupling scheme by extending Eq. (3) as[23,24]

$$\mathbf{N} = \mathbf{N}_a + \mathbf{N}_b, \quad \mathbf{J} = \mathbf{N} + \boldsymbol{l}, \quad \mathbf{J}_T = \mathbf{J} + \mathbf{S} \tag{13}$$

and express the corresponding eigenbasis in terms of the spin-free basis elements, Eq. (4),

$$|((N_a N_b) Nl) JS; J_T M_T\rangle = \sum_{M, m_S} C^{JSJ_T}_{M m_S M_T} |(N_a N_b) Nl; JM\rangle \otimes |S m_S\rangle . \tag{14}$$

The use of Eq. (14) as the expansion basis for the total wave function is more convenient as far as the close-coupling calculations are concerned. Namely, if the collisional energies E considered in the scattering calculations are large compared with the fine structure splitting of rotational levels of O_2, one may neglect in $\mathcal{H}^{(a)}$ interactions involving electronic spin and consider only the rotational term $\mathcal{H}_{\rm rot}^{(a)}$. Furthermore, if the interaction potential V is assumed spin-independent, the only operators in the Hamiltonian acting on spin eigenstates in Eq. (14) are identity maps and from the computational point of view the $O_2(^3\Sigma_g^-)$–$N_2(^1\Sigma_g^+)$ collisional problem is reduced to the simpler case of scattering between two rigid rotors in $^1\Sigma$ electronic states. One may therefore solve the regular close-coupling equations, Eq. (6), and extract the spin-free S-matrix elements from Eq. (7).

In pressure broadening calculations however, the goal is to study the effect of the bath (characterized by $\mathbf{j}_R$) on the optical transitions of the spectroscopically active O_2 molecule, the states of which, from the experimental point of view, should be labeled by $|(N_a S) jm\rangle$. Hence, when considering the shapes of molecular O_2 resonances in the N_2 bath, the use of coupled states defined in Eq. (12) is preferred. The representation of the S-matrix in the spectroscopic basis from Eq. (12) may then be obtained by establishing a transformation between Eqs. (12) and (14). It is shown in the Appendix that the unitary change of basis is given by

$$\begin{aligned} &|(N_b l) j_R (N_a S) j; J_T M_T\rangle = \\ &(-1)^{N_a + N_b + l + S + J_T} \sum_{J,N} \left[j, j_R, J, N\right]^{\frac{1}{2}} \begin{Bmatrix} j_R & N_a & J \\ S & J_T & j \end{Bmatrix} \\ &\times \begin{Bmatrix} N_a & N_b & N \\ l & J & j_R \end{Bmatrix} |((N_a N_b) Nl) JS; J_T M_T\rangle , \end{aligned} \tag{15}$$

which allows one to obtain the S-matrix elements in the spectroscopic representation:

$$\begin{aligned} &\hat{\rm S}^{J_T}_{(N'_b l') j'_R (N'_a S) j', (N_b l) j_R (N_a S) j} = (-1)^{N_b + N'_b + l + l'} \\ &\times \left[j_R, j'_R, j, j'\right]^{\frac{1}{2}} \sum_{J,N,N'} \left[J\right] \left[N, N'\right]^{\frac{1}{2}} \begin{Bmatrix} N_a & N_b & N \\ l & J & j_R \end{Bmatrix} \\ &\times \begin{Bmatrix} N'_a & N'_b & N' \\ l' & J & j'_R \end{Bmatrix} \begin{Bmatrix} j_R & N_a & J \\ S & J_T & j \end{Bmatrix} \begin{Bmatrix} j'_R & N'_a & J \\ S & J_T & j' \end{Bmatrix} \\ &\times \hat{\rm S}^{J}_{(N'_a N'_b) N' l', (N_a N_b) Nl} , \end{aligned} \tag{16}$$

where a shorthand notation $[x, ..., z] = (2x+1)...(2z+1)$ is introduced, and $\left\{ \cdot \cdot \cdot \right\}$ is the $6j$ symbol.[13] Equations (15) and (16) differ from that given originally by Alison Offer *et al.*[24] in the phase factors. This is of some importance, since phases of the form $(-1)^{2K}$ may be omitted only when K in an integer – for K half-integer, e.g. spin 1/2, then $(-1)^{2K} = -1$, and some expressions change sign.

If a transition occurs between the fine structure levels of O_2 during the collision, the influence of the nitrogen bath on a particular spectral line may be accounted for by using the S-matrices obtained from Eq. (16) to compute the pressure broadening cross sections. The latter are given, in the present case, by the real part of the complex

quantity[67]

$$\sigma_0^{(q)}(N_{a_i}j_i, N_{a_f}j_f; N_b|E_k) = \frac{\pi}{k^2}\sum_{N_b'}\sum_{J_T,\bar{J}_T}\sum_{\substack{l,l',\\ j_R,j_R'}}(-1)^{j_R+j_R'} \times\left[J_T,\bar{J}_T\right]\begin{Bmatrix} j_i & j_f & q\\ \bar{J}_T & J_T & j_R'\end{Bmatrix}\begin{Bmatrix} j_i & j_f & q\\ \bar{J}_T & J_T & j_R\end{Bmatrix}\Big(\delta_{N_bN_b'}\delta_{ll'}\delta_{j_Rj_R'} -\hat{\mathrm{S}}^{J_T}_{(N_b'l')j_R'N_{a_i}j_i,(N_bl)j_RN_{a_i}j_i}\,\hat{\mathrm{S}}^{\bar{J}_T*}_{(N_b'l')j_R'N_{a_f}j_f,(N_bl)j_RN_{a_f}j_f}\Big), \tag{17}$$

where $\{N_{a_i}, j_i\}$ and $\{N_{a_f}, j_f\}$ are the angular momentum quantum numbers of the initial and final spectroscopic states of O_2, respectively, and line mixing is neglected (i.e., it is assumed that $\{N_{a_i}, j_i\} = \{N'_{a_i}, j'_i\}$ and $\{N_{a_f}, j_f\} = \{N'_{a_f}, j'_f\}$). The quantum numbers corresponding to the 118 GHz fine structure $1-$ line in O_2 are $N_{a_i} = N_{a_f} = 1$, $j_i = 1$ and $j_f = 0$; the electronic spin quantum number $S = 1$ is omitted.

In Eq. (17), both S-matrices are calculated at the same relative kinetic energy of the colliding monomers, which is defined as

$$E_k = E - (E^{(a)}_{\mathrm{rot}} + E^{(b)}_{\mathrm{rot}}). \tag{18}$$

For the magnetic dipole transition considered here, the rank of the radiation-matter interaction tensor is $q = 1$.

III. POTENTIAL ENERGY SURFACE

The non-bonded interaction energies were computed using explicitly-correlated unrestricted coupled-cluster theory[68] with all electrons (AE) correlated, extrapolated to the complete basis set limit, (AE)UCCSD(T)-F12b/CBS. The basis extrapolation was performed using the Peterson CVTZ-F12 and CVQZ-F12 bases[69] and the l^{-3} formula.[70] All *ab initio* calculations were performed using the MOLPRO electronic structure code package.[71] Stable convergence to the restricted open-shell Hartree–Fock (roHF) reference was achieved by first using MOLPRO's CASSCF (multi) algorithm with the occupation of the desired configuration specified, followed by a single iteration of the roHF SCF algorithm to prepare the orbitals for the UCCSD(T)-F12b procedure. A *geminal beta* coefficient value of 1.5 was specified for the all-electron F12 calculations. For construction of the four-dimensional PES, both monomers were held rigid. The r(N–N) bond length was fixed at 1.0975 Å, consistent with its rotational constant, $B = 1.98950$ cm^{-1}.[72] The geometry of the O_2 molecule was held at equilibrium, using the vibrationally averaged distance: r(O–O)= 1.20752 Å, which is also consistent with its experimental rotational constant.[73] Exploiting the system's symmetry, energies were only computed in a reduced angular range: $0 < \vartheta_a < 90$, $0 < \vartheta_b < 90$, and $0 < \phi < 180$.

As we have done in the past for other van der Waals dimers composed of linear monomer fragments,[74–85] an analytical representation of the PES was constructed using an automated interpolating moving least squares (IMLS) methodology, which is available as a software package under the name AUTOSURF.[86] As usual,[87,88] a local fit was expanded about each data point, and the final potential is obtained as the normalized weighted sum of the local fits. This interpolative approach can accommodate arbitrary energy-surface topographies and is particularly advantageous in cases of PESs with large anisotropy.

The shortest intermonomer center-of-mass distance considered is $R = 2.0$ Å. The *ab initio* data coverage in the fitted PES extends to $R = 20.0$ Å, while the zero of energy is set at infinite center-of-mass separation between the monomers. The fitting basis and other aspects of the procedure were the same as for other previous systems and have been described in detail elsewhere.[79,86,88] The global estimated root-mean-squared (RMS) fitting error tolerance was set below 0.2 cm^{-1} for energies below the asymptote, and the total number of automatically generated symmetry-unique points needed to reach that target was 1260. The actual RMS error (for energies below the asymptote) was evaluated as 0.159 cm^{-1}. As expected for a system whose leading electrostatic interaction term is quadrupole–quadrupole, the well-depth is modest, and the PES is quite flat beyond $R = 10.0$ Å.

The global minimum (GM) is cross-shaped, with $\phi = 90°$. The upper panel of Fig. 2 shows a 2D representation of the PES (denoted R-optimized) as a function of the angles ϑ_a and ϑ_b for configurations with $\phi = 90°$. The plot describes the complete ranges of ϑ_a and ϑ_b, relaxing the intermonomer distance coordinate R for each pair of angles. The position of stationary points and the corresponding molecular configurations of the system are also highlighted in the figure. The cross-shaped GM appears in the center of the figure. A low energy channel stretches vertically in the plot. Motion along this channel involves rotation of the N_2 fragment (in the plane of the figure) changing ϑ_b, and reaching a T-shaped transition structure (TS2) at the bottom of the figure, or equivalently at the top. In this T-shaped transition structure, the N_2 fragment serves as the stem, pointing into the middle of the O_2 molecule. Rotating ϑ_b a full 180°, brings the system back to the global minimum in the center. Rotating the O_2 fragment, changing ϑ_a, is quite different, passing through a transition structure (TS1) before reaching the other T-shaped structure (with O_2 as the stem) which in this case is a local minimum (LM).

Beginning at the global minimum, rotation in ϕ brings the system through a planar configuration ($\phi = 0°$), before returning to the global minimum after a full 180° rotation. This planar configuration is a third transition structure (TS3). The lower panel of Fig. 2 shows the corresponding ϑ_a and ϑ_b plot (relaxed in R), for planar geometries ($\phi = 0°$). TS3, the side-by-side parallel structure appears in the center of the plot. Again in this plane, rotation of N_2 (ϑ_b) is very facile with a low energy channel leading to the T-shaped TS2 at the top and bot-

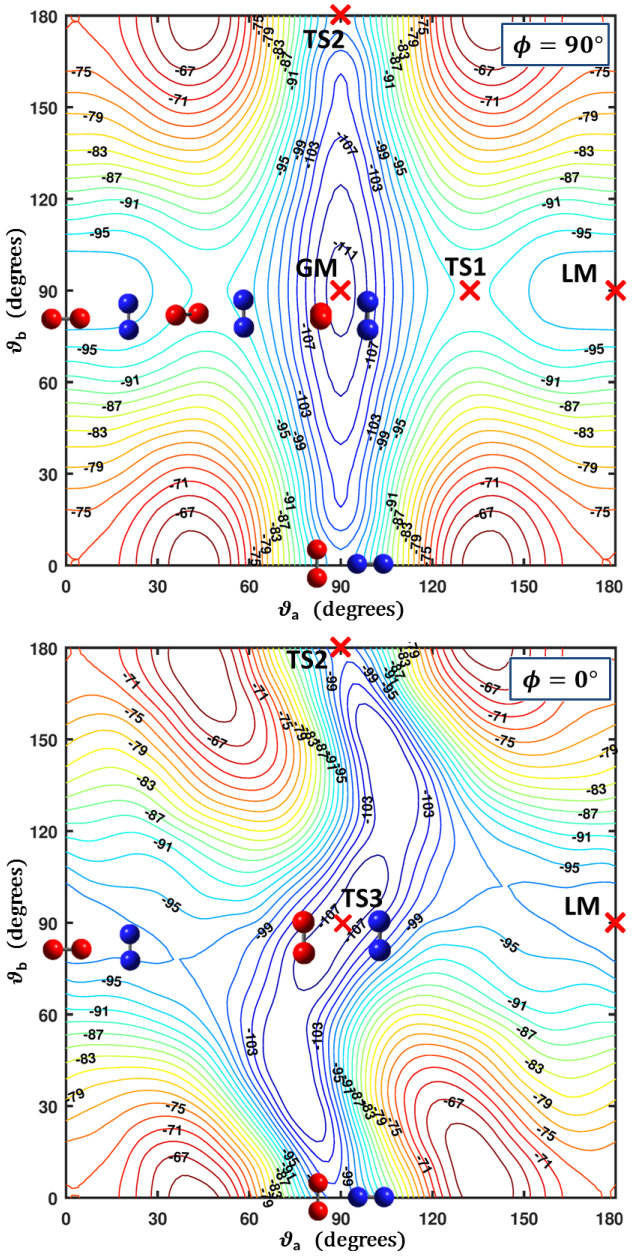

FIG. 2. (upper panel) R-optimized contour plot of the PES as a function of the angles ϑ_a and ϑ_b, with the torsion fixed at $\phi = 90°$. For each pair of angles, the energy (given in cm^{-1}) is optimized with respect to the center-of-mass distance R. The global minimum appears at the center of the plot. Two transition structures and a local minimum also appear in the plot (see text). (lower panel) The corresponding plot for planar configurations with $\phi = 0°$ is given. A third transition structure is found at the center (see text).

tom of the figure (appearing also in the plot in the upper panel).

Geometric parameters of the critical points (including the two minima and three transition structures) are given in Table I. As can be seen in the table, the well-depth of the global minimum is 112.0 cm^{-1}, but the system is very flexible, with long low-energy channels available in multiple directions. Indeed, two of the TS are lower in energy than the local minimum. We have characterized the features of the PES here in terms of minima and transition structures, but note that rovibrational bound states would exhibit extensive delocalization.A previously reported PES was constructed by Bartolomei *et al.*[41] in 2014 based on SAPT(DFT) methodology. The global minimum on the SAPT PES is also cross-shaped, and has a very similar inter-monomer distance ($R = 3.45$ Å), but slightly larger well-depth (118 cm^{-1}). Our new PES is expected to be more accurate, but with both PESs in hand, more detailed comparisons including analysis of the bound states of the complex is a possible future avenue of investigation.

TABLE I. Geometric parameters and potential energy for equilibrium and transition structures as shown in Fig. 2. Energies are given relative to the asymptote ($V_{\rm abs}$) and also relative to the global minimum ($V_{\rm rel}$) of the PES. Units are angströms, degrees, and cm^{-1}.

	GM	LM	TS1	TS2	TS3
R	3.435	3.918	3.779	3.944	3.459
ϑ_a	90.0	0.0	47.4	90.0	90.0
ϑ_b	90.0	90.0	90.0	0.0	90.0
ϕ	90.0	–	90.0	–	0.0
$V_{\rm abs}$	-112.0	-98.8	-94.8	-100.4	-107.9
$V_{\rm rel}$	0.0	13.2	17.2	11.6	4.1

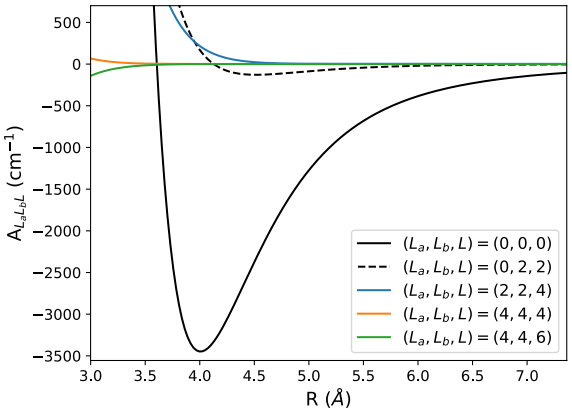

FIG. 3. The isotropic (black solid line) and the leading anisotropic (dashed line) radial terms of the PES in the vicinity of the isotropic term's minimum, with further anisotropic contributions given by the colored solid lines, for reference. Note that the curves are normalized according to Eq. (22).

To evaluate the potential matrix elements in Eq. (6),

the radial and angular parts of the PES are separated:

$$V(R,\vartheta_a,\vartheta_b,\phi)=\sum_{L_a,L_b,L} A_{L_aL_bL}(R)I_{L_aL_bL}(\vartheta_a,\vartheta_b,\phi), \tag{19}$$

where[39]

$$I_{L_aL_bL}(\vartheta_a,\vartheta_b,\phi)=\sqrt{\frac{2L+1}{4\pi}}\sum_{\mu} C^{L_aL_bL}_{\mu-\mu0} \times Y_{L_a\mu}(\vartheta_a,\varphi_a)Y_{L_b-\mu}(\vartheta_b,\varphi_b) \tag{20}$$

are the bispherical harmonics, $A_{L_aL_bL}(R)$ are the radial terms of the potential and the corresponding coordinates are defined in Fig. 1. Here $Y_{L_i\mu_i}(\vartheta_i,\varphi_i)$ denotes the usual spherical harmonic function,[13] and L_a and L_b take non-negative even integer values (which follows from O_2 and N_2 being homonuclear species).[25] Additionally $|L_a-L_b|\le L\le L_a+L_b$ and the sum of these three indices must be an even integer.[39] Expressed in terms of the radial coefficients $A_{L_aL_bL}(R)$, the potential matrix elements in the close-coupling equations take the form

$$\begin{aligned} V^J_{(N'_aN'_b)N'l',(N_aN_b)Nl} &= [N_a,N_b,N,l,N'_a,N'_b,N',l']^{\frac{1}{2}} \\ &\times(4\pi)^{-\frac{3}{2}}(-1)^{J+N+N'_a+N'_b}\sum_{L_a,L_b,L}[L][L_a,L_b]^{\frac{1}{2}} \\ &\times\begin{pmatrix} N'_a & L_a & N_a\\ 0 & 0 & 0\end{pmatrix}\begin{pmatrix} N'_b & L_b & N_b\\ 0 & 0 & 0\end{pmatrix}\begin{pmatrix} N' & L & N\\ 0 & 0 & 0\end{pmatrix} \\ &\times\begin{Bmatrix} l & N & J\\ N' & l' & L\end{Bmatrix}\begin{Bmatrix} N' & N & L\\ N'_a & N_a & L_a\\ N'_b & N_b & L_b\end{Bmatrix}A_{L_aL_bL}(R), \end{aligned} \tag{21}$$

where $\left\{\begin{smallmatrix}\cdot&\cdot&\cdot\\ \cdot&\cdot&\cdot\\ \cdot&\cdot&\cdot\end{smallmatrix}\right\}$ is a $9j$ symbol.[13,89]

The radial terms of the potential are obtained by integrating Eq. (19) over the angular distribution:[39,41]

$$A_{L_aL_bL}(R)=\frac{8\pi^2}{2L+1}\int_0^{2\pi}\mathrm{d}\phi\int_{-1}^{1}\mathrm{d}(\cos\theta_a)\int_{-1}^{1}\mathrm{d}(\cos\theta_b) \times V(R,\vartheta_a,\vartheta_b,\phi)I_{L_aL_bL}(\vartheta_a,\vartheta_b,\phi). \tag{22}$$

In the present work we use a 19-point Gauss-Legendre quadrature for performing the integration over all angles in order to ensure the normalization of the bispherical harmonics. 85 radial terms in total were prepared, with the maximum (L_a,L_b,L) triad being $(8,8,16)$, and the radial grid consisted of 901 points spanning from 2.6 Å to 26.5 Å, which we obtained by using the fitted form of the PES. The isotropic A_{000} and the leading anisotropic A_{022} radial terms are presented in Fig. 3, together with sample anisotropic radial contributions; it can be seen that the isotropic term dominates in the expansion.

TABLE II. Rotational energies (in cm^{-1}) of O_2 and N_2 used in the construction of the computational basis for the scattering calculations.

N_a	$E^{(a)}_{\mathrm{rot}}$	N_b	$E^{(b)}_{\mathrm{rot}}$
1	2.8753	0	0.0000
3	17.2512	1	3.9781
5	43.1253	2	11.9342
7	80.4935	3	23.8680
9	129.3497	4	39.7791
11	189.6861	5	59.6670
13	261.4929	6	83.5309
15	344.7585	7	111.3700
17	439.4694	8	143.1835
19	545.6103	9	178.9700
21	663.1640	10	218.7285

IV. SCATTERING CALCULATIONS

To obtain the S-matrix elements in the spectroscopic representation we use the evaluated radial terms of the PES to solve the spin-free close-coupling equations, Eq. (6), and match their asymptotic solutions to the boundary condition, Eq. (7). The calculations were performed using a newly developed BIGOS code,[90] which implements the renormalized Numerov's propagator.[91]

For binary collisions between diatomic molecules typical for Earth's atmosphere, the $\{|N_am_a\rangle,|N_bm_b\rangle\}$ basis size used in the calculations grows considerably with E_k, the relative kinetic energy of the monomers.[39] To reduce the number of basis elements necessary for the convergence of numerical calculations, we made use of the fact that the non-zero spin of the ^{14}N nuclei gives rise to the two isomers of molecular nitrogen (*ortho*-N_2, for which the total nuclear spin $I=0,2$ and only even N_b values occur; and *para*-N_2, for which $I=1$ and only odd values of N_b occur). Thus the scattering calculations are performed independently for the O_2–*ortho*-N_2 and O_2–*para*-N_2 systems. The rotational energies used in the construction of the computational basis are presented in Table II; the energies of the O_2 monomer were obtained from the effective Hamiltonian[26] as

$$E^{(a)}_{\mathrm{rot}}=B_aN_a(N_a+1)-D_aN_a^2(N_a+1)^2, \tag{23}$$

where the rotational and centrifugal distortion constants are taken,[26] respectively, as $B_a=1.438\ \mathrm{cm}^{-1}$ and $D_a=4.84\times10^{-6}\ \mathrm{cm}^{-1}$; and the energies of N_2 are taken from the HITRAN database.[92]

The total collisional energy E determined the proper basis size to include two asymptotically closed levels (i.e., levels for which $E<E^{(a)}_{rot}+E^{(b)}_{rot}$) throughout the calculations. For *ortho*-N_2, this corresponded to $M\le8$ for kinetic energies up to 50 cm^{-1}, $M\le14$ for kinetic energies up to 100 cm^{-1}, $M\le16$ for kinetic energies up to 125 cm^{-1} and $M\le20$ for kinetic energies up to

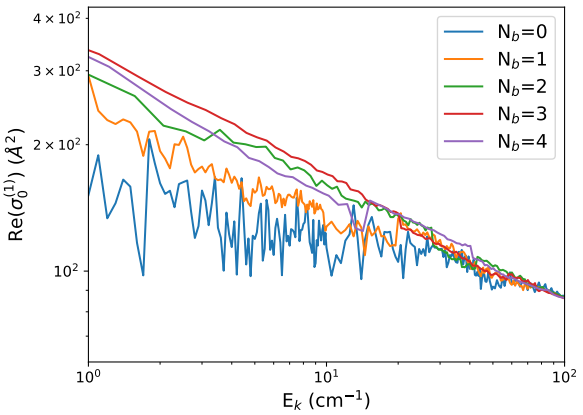

FIG. 4. Pressure broadening cross sections for the first five rotational levels of the perturber.

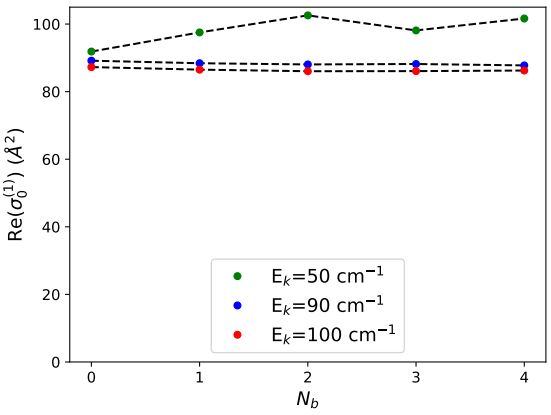

FIG. 5. Dependence of the pressure broadening cross sections on the perturber's rotational quantum number N_b. Following the behaviour in higher kinetic energies, the cross sections for $N_b > 4$ were extrapolated with their values at $N_b = 4$.

150 cm^{-1}. Similarly, for *para*-N_2 $M \leq 9$ for kinetic energies up to 50 cm^{-1}, $M \leq 16$ for kinetic energies up to 100 cm^{-1}, $M \leq 18$ for kinetic energies up to 125 cm^{-1} and $M \leq 21$ for kinetic energies up to 150 cm^{-1}.

The radial grid for the propagation is set, in both cases, from 2.6 Å to 26.5 Å and the propagation step is set to 35 steps per half de Broglie wavelength. The spin-free calculations are performed for the total angular momentum J ranging, with step size set to 1, from $J_{\min} = 0$ up to $J_{\max}$ which was determined by the convergence criterion, namely that the contributions to the elastic and inelastic cross sections calculated for four consecutive values of J were smaller than 10^{-3}.

The spin-free S-matrix elements obtained from the scattering calculations are transformed to the spectroscopic representation with the use of Eq. (16), and used in the evaluation of the generalized spectroscopic cross sections, Eq. (17). In this work we focus on the pressure broadening cross section, which is given by the real part of $\sigma_0^{(1)}$. Figure 4 presents the dependence of Re($\sigma_0^{(1)}$) on the collisional kinetic energy for several values of the rotational quantum number N_b of the perturbing molecular nitrogen. It can be seen that for large relative kinetic energies the cross sections become state-independent and approximately the same power-law behaviour is observed for all rotational states. This may be qualitatively accounted for by noting that the O_2–N_2 interaction is mostly isotropic (see Fig. 3), which allows the molecular collisions to sample the same repulsive short-range part of the PES for sufficiently large collision kinetic energy. This observation is made more evident by analyzing the cross sections' N_b-dependence presented in Fig. 5. Since for $N_b > 4$ there is almost no further dependence of the pressure broadening cross sections on the rotational state of the perturber, we assume the values of Re($\sigma_0^{(1)}$) for $N_b > 4$ to be the same as for $N_b = 4$.

In order to compute the *ab initio* collision integrals necessary to evaluate the line shape parameters for the perturbed molecular transition, the generalized spectroscopic cross section has to be calculated in a wide range of kinetic energies. Since the O_2–N_2 system is computationally expensive as far as the approximation-free close-coupling simulations are concerned, we were able to perform the scattering calculations up to an E_k of approximately 150 cm^{-1}. In Figure 4, a power-law behaviour is observed for cross sections above $E_k \sim 60$ cm^{-1}, which allows us to extrapolate them at higher kinetic energies by using the power-law function

$$\sigma_0^{(1)}(E_k) = A\left(\frac{E_0}{E_k}\right)^b, \tag{24}$$

where $E_0 = 100$ cm^{-1} is a reference kinetic energy. The parameters A and b are obtained, for each rotational state of the perturber, by fitting Eq. (24) to the calculated values of $\sigma_0^{(1)}(E_k)$ in the range $E_{\text{cutoff}} \leq E_k \leq E_{\max}$, where E_{cutoff} is the cutoff energy chosen depending on the value of N_b, and $E_{\max}$ is the largest kinetic energy attained in the *ab initio* calculations.

Table III gives the values of the fitted power-law parameters together with the corresponding cutoff energies, and a sample extrapolation is presented in Fig. 6. Due to the pronounced state-dependence of the low-energy cross sections observed in Fig. 4, in the line-shape calculations we use the *ab initio* values for $\sigma_0^{(1)}(E_k \leq E_{\text{cutoff}})$; following the cutoff energies, the cross sections are extrapolated with use of Eq. (24) up to $E_k \sim 4000$ cm^{-1}.

V. PRESSURE BROADENING OF THE N_2-PERTURBED 118 GHZ LINE IN O_2

The speed-averaged pressure broadening coefficient γ_0 quantifying the half-width of the shape of a given

TABLE III. The cutoff energies $E_{\rm cutoff}$ (in cm^{-1}) for the numerical fit of Eq. (24), and the fitted power-law parameters A and b (the uncertainty of the numerical fit is given in parentheses).

N_b	$E_{\rm cutoff}$	A	b
0	130.00	86.19(5)	0.267(2)
1	110.00	87.08(9)	0.312(8)
2	113.07	86.09(7)	0.240(5)
3	90.11	86.08(4)	0.230(7)
4	60.22	86.2(3)	0.22(1)

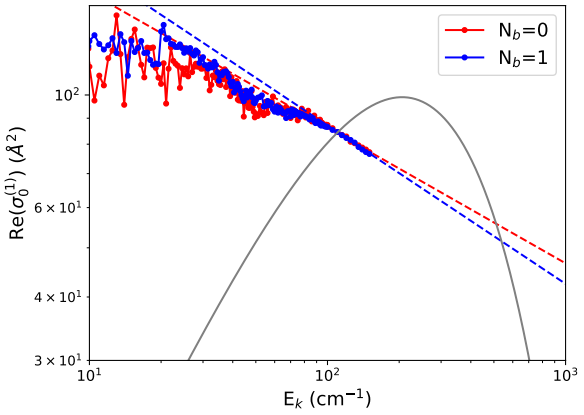

FIG. 6. The *ab initio* (solid lines) and extrapolated (dashed lines) values of Re($\sigma_0^{(1)}$) obtained by fitting the power law in Eq. (24). The Maxwell–Boltzmann distribution at 296 K (gray line) is plotted, in arbitrary units, for reference.

$\{N_{a_i}, j_i\} \rightarrow \{N_{a_f}, j_f\}$ molecular resonance is obtained with use of the broadening cross sections, Eq. (17), as[39,93]

$$\gamma_0 = \frac{1}{2\pi c}\frac{\bar{v}_r}{k_B T}\sum_{N_b} p_{N_b}\,\mathrm{Re}\int_0^\infty \mathrm{d}x x e^{-x}\sigma_0^{(q)}(N_{a_i}j_i, N_{a_f}j_f; N_b|x), \tag{25}$$

where $x = E_k/k_BT$, k_B and T are the Boltzmann constant and gas temperature, respectively, and $\bar{v}_r = \sqrt{8k_BT/\pi\mu}$ is the mean relative speed of the monomers; the $(2\pi)^{-1}$ factor arises when one expresses the spectrum in units of frequency, ν, and not angular frequency, ω, and the $1/c$ factor converts the frequency units into wave numbers.[93]

The statistical weights p_{N_b} give the probability of the perturbing molecule being, at a given temperature T, in a rotational state of energy $E_{\rm rot}^{(b)}$ characterized by the quantum number N_b:

$$p_{N_b} = \frac{1}{Z(T)} w_{N_b}(2N_b+1)e^{-E_{\rm rot}^{(b)}/k_BT}, \tag{26}$$

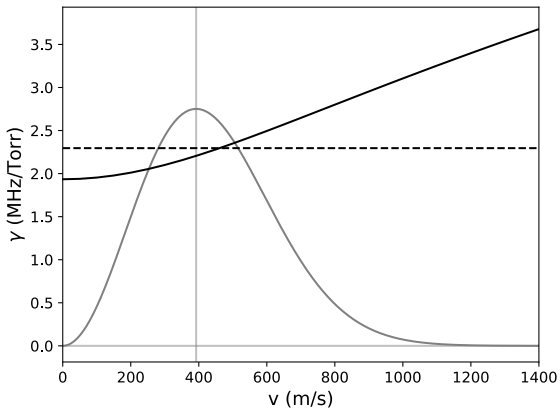

FIG. 7. *Ab initio* speed-dependent pressure broadening coefficient $\gamma(v)$ (black solid line) for the N_2-perturbed 118 GHz fine structure line of O_2 at 296 K and the speed-averaged broadening parameter γ_0 (dashed line). For reference, the speed distribution of the O_2 molecule (gray solid line) at 296 K is presented in arbitrary units.

where

$$Z(T) = \sum_{N_b} w_{N_b}(2N_b+1)e^{-E_{\rm rot}^{(b)}/k_BT} \tag{27}$$

is the partition function and w_{N_b} are the weights associated with the nuclear spin degeneracy of each rotational level – in the present case of perturbations by the N_2 molecule, to its *ortho* and *para* species correspond $w_{N_b} = 6$ and $w_{N_b} = 3$, respectively (see the discussion in Section IV). In order to cover the 99% of the rotational population of N_2 at room temperature (296 K) we extended the summation in Eq. (27) up to the rotational level with $N_b = 31$.

In a more realistic approach, one includes the dependence of the collisional broadening on the speed v possessed by the spectroscopically active molecule by replacing Eq. (25) with its speed-dependent counterpart[93]

$$\gamma(v) = \frac{1}{2\pi c}\frac{1}{k_BT}\frac{2}{\sqrt{\pi}v_p v}\sum_{N_b} p_{N_b}\,\mathrm{Re}\int_0^\infty \mathrm{d}v_r v_r^2 \sinh\left(\frac{2vv_r}{v_p^2}\right) \times e^{-\frac{v^2+v_r^2}{v_p^2}}\sigma_0^{(q)}(N_{a_i}j_i, N_{a_f}j_f; N_b|v_r), \tag{28}$$

where $v_p = \sqrt{2k_BT/m_b}$ is the most probable speed of the perturber of mass m_b and the integration is over the relative speeds v_r of the two molecules. The speed-dependent broadening coefficient $\gamma(v)$ at 296 K is plotted in Fig. 7 against the corresponding Maxwell–Boltzmann distribution, which determines the value of γ_0 also shown for comparison.

In order to determine the effective broadening of the spectral line, which takes into account the speed dependence of γ, we simulate the line shape with the weighted

TABLE IV. Available experimental and *ab initio* values of pressure broadening coefficients for the 118 GHz line in O_2 perturbed by N_2. The uncertainties of our results in parentheses correspond to the estimated 4% accuracy of the calculations for γ, and to the uncertainty of the numerical fit of Eq. (30) for n_γ.

Experiment	T (K)	γ (MHz/Torr)	n_γ
Pickett *et al.*[19]	207	2.83(6)	–
	281	2.38(5)	–
	295	2.2(1)	–
Golubiatnikov *et al.*[20]	297	2.245(20)	–
Drouin[21]	296	2.06(6)	1.00(5)
Makarov *et al.*[15]	300	2.255(14)	0.79(5)
Koshelev *et al.*[16]	296	2.278(2)	0.781(6)
This work, WSLP	296	2.28(9)	0.7231(1)
This work, γ_0	296	2.30(9)	0.7245(6)

sum of Lorentz profiles (WSLP):[28]

$$\mathcal{I}_{WSLP}(\omega-\omega_0') = \frac{1}{\pi}\int \mathrm{d}^3\vec{v} f_m(\vec{v}) \frac{\gamma(v)}{\gamma^2(v)+(\omega-\omega_0')^2}, \tag{29}$$

where $f_m(\vec{v})$ is the Maxwell–Boltzmann distribution of the active molecule's velocity and ω_0' is the line position including the eventual speed-dependent shift that we disregard here. We then fit the obtained *ab initio* points with the usual Lorentzian profile thus being able to determine the half-width at half-maximum (HWHM) of the fitted line shape. The speed dependence of γ results in the effective width of the line being smaller than that given by the speed-averaged coefficient γ_0;[39] hence it is the WSLP simulation that is compared with the experiment.

The speed-averaged and WSLP broadening coefficients were calculated for several temperatures in the range 200–400 K, and the *ab initio* points thus obtained were fitted with the power law

$$\gamma(T) = \gamma(T_0)\left(\frac{T_0}{T}\right)^{n_\gamma}, \tag{30}$$

where T_0 is a reference temperature, in our case 296 K, and n_γ is the fitted temperature exponent. A comparison between the theoretically predicted temperature dependence of the collisional broadening and the experimental results[15,16,19,21] is given in Fig. 8. The mentioned narrowing of the line shape due to the speed dependence of γ can be observed. The shaded region corresponds to the uncertainty of our WSLP simulation results, which we estimate at 4% based on considerations described in our previous works.[31,35,39] Table IV gives the numerical values of experimental half-widths γ and our *ab initio* results.

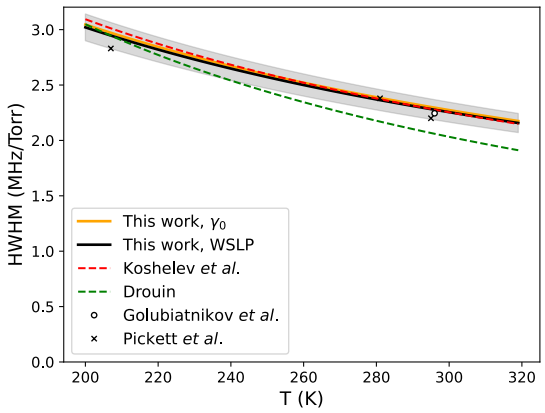

FIG. 8. Comparison between the *ab initio* (solid lines) and experimental temperature dependence of the pressure broadening for the 118 GHz oxygen line perturbed by N_2. The shaded region corresponds to the estimated 4% uncertainty of the WSLP results. The corresponding references to the experimental papers are given in Table IV.

VI. CONCLUSION

In this paper, we presented the first calculations of the $O_2(^3\Sigma_g^-)$–$N_2(^1\Sigma_g^+)$ scattering in the context of fine structure lines of O_2. We computed a new *ab initio* O_2–N_2 PES on which fully quantum dynamical calculations were performed. By changing the representation basis of the scattering matrix, we calculated the pressure broadening cross sections for the fine structure 118 GHz transition in O_2 occurring within a single rotational level. Our treatment of collision dynamics is based fully on the close-coupling approach, and no further dynamical approximations were made. We calculated the effective collisional half-widths of the N_2-perturbed 118 GHz fine structure line of O_2 and provided its temperature dependence over the 200–400 K range. We obtained a good agreement with the available experimental data. This study is the first step towards the accurate theoretical study of collisional perturbations of the fine structure and rotational lines of $O_2(^3\Sigma_g^-)$ due to molecular species of atmospheric importance, such as N_2. Such investigations are of great importance for the Earth's atmosphere studies and remote sensing, and populating spectroscopic databases (such as HITRAN or GEISA) with accurate theoretical values of line-shape parameters. This first work paves the route for further studies that will include the couplings between the lines that affect the pure rotational band shape.

SUPPLEMENTARY MATERIAL

See the supplementary material associated with this article for the tabulated radial terms of the O_2–N_2 PES

and the pressure broadening cross sections used in the line-shape calculations.

ACKNOWLEDGMENTS

M.G., H.J. and P.W. are supported by the National Science Centre in Poland through Project No. 2018/31/B/ST2/00720. R.D. and E.Q.-S. are supported by the U.S. Department of Energy (Award DE-SC0019740). This project is supported by the French-Polish PHC Polonium program (Project No. 42769ZK for the French part). This project is co-financed by the Polish National Agency for Academic Exchange under the PHC Polonium program (Grant No. dec. PPN/X/PS/318/2018). This research is a part of the program of the National Laboratory FAMO in Toruń, Poland.

AUTHOR DECLARATIONS

Conflict of interest

The authors have no conflicts to disclose.

DATA AVAILABILITY

The data that supports the findings of this study are available within the article and its supplementary material.

Appendix: Change of basis

One can derive the formula for the change of basis, Eq. (15), by the successive recoupling of angular momenta used to label the bases of the two representations. To do so, one first recouples $\mathbf{j}_R$ and $\mathbf{N}_a$ to produce $\mathbf{J}$ (see Eq. (11) and Eq. (13)), leading to the spectroscopic-basis ket[13,26]

$$|(N_b l) j_R (N_a S) j; J_T M_T\rangle = \sum_J (-1)^{j_R+N_a+S+J_T} [J,j]^{\frac{1}{2}} \times \begin{Bmatrix} j_R & N_a & J \\ J_T & S & j \end{Bmatrix} |((N_b l) j_R N_a) J S; J_T M_T\rangle \,. \tag{A.1}$$

In order to recover the same labeling as in the scattering basis vector, Eq. (14), one needs to change the order of j_R and N_a in the rightmost ket in Eq. (A.1),

$$|((N_b l) j_R N_a) J S; J_T M_T\rangle = (-1)^{j_R+N_a-J} |(N_a (N_b l) j_R) J S; J_T M_T\rangle \,, \tag{A.2}$$

where an additional phase factor is due to the property $|(j_1 j_2) j_{12}\rangle = (-1)^{j_1+j_2-j_{12}} |(j_2 j_1) j_{12}\rangle$, which follows from the symmetry properties of Clebsch-Gordan coefficients.[13,89]

Upon recoupling N_a and N_b to N (see Eq. (13)) and making use of Eq. (A.1), one may write

$$|(N_b l) j_R (N_a S) j; J_T M_T\rangle = (-1)^{N_a+N_b+l+S+J_T} \sum_{J,N} [j, j_R, J, N]^{\frac{1}{2}} \begin{Bmatrix} j_R & N_a & J \\ S & J_T & j \end{Bmatrix} \times \begin{Bmatrix} N_a & N_b & N \\ l & J & j_R \end{Bmatrix} |((N_a N_b) N l) J S; J_T M_T\rangle \,, \tag{A.3}$$

thus proving Eq. (15). Note that in the above the phase term $(-1)^{2j_R+2N_a}$ is omitted, since j_R and N_a are both integers.

Now, recall the definition of the spin-free representation in Eq. (14). Considering that the interaction is assumed to be independent of the electronic spin and that in the Hund's case (b) the coupling between the rotational angular momentum and spin is weak,[23] S acts as a "spectator during the collision".[60,61] Consequently, the S-matrix does not act on the spin eigenstates $|S m_S\rangle$. Hence the transformation in Eq. (A.3) and the orthogonality of the Clebsch-Gordan coefficients result in the relationship between the spectroscopic and spin-free representations of the S-matrix:

$$\hat{\mathrm{S}}^{J_T}_{(N_b' l') j_R' (N_a' S) j', (N_b l) j_R (N_a S) j} = (-1)^{N_a+N_a'+2(S+J_T)} \times (-1)^{N_b+N_b'+l+l'} [j_R, j_R', j, j']^{\frac{1}{2}} \sum_{J,N,N'} [J][N,N']^{\frac{1}{2}} \times \begin{Bmatrix} N_a & N_b & N \\ l & J & j_R \end{Bmatrix} \begin{Bmatrix} N_a' & N_b' & N' \\ l' & J & j_R' \end{Bmatrix} \begin{Bmatrix} j_R & N_a & J \\ S & J_T & j \end{Bmatrix} \times \begin{Bmatrix} j_R' & N_a' & J \\ S & J_T & j' \end{Bmatrix} \hat{\mathrm{S}}^J_{(N_a' N_b') N' l', (N_a N_b) N l} \,. \tag{A.4}$$

Observe that, for the case of $\mathrm{O}_2(^3\Sigma_g^-)$, N_a and N_a' are odd – therefore the phase $(-1)^{N_a+N_a'} = +1$, and hence may be omitted. Furthermore, since the total spin-free angular momentum J is an integer, adding a $(-1)^{2J}$ factor under the summation does not change anything, and we obtain in this way the effective phase $(-1)^{2(S+J_T+J)}$. Now, the sum $S + J_T + J$ is an integer because the three quantum numbers are connected by the $6j$ symbol;[13] therefore $(-1)^{2(S+J_T+J)} = +1$ may be omitted and we

obtain the simplified expression

$$\hat{\mathrm{S}}^{J_T}_{(N_b'l')j_R'(N_a'S)j',(N_bl)j_R(N_aS)j} = (-1)^{N_b+N_b'+l+l'} \times [j_R, j_R', j, j']^{\frac{1}{2}} \sum_{J,N,N'} [J][N,N']^{\frac{1}{2}} \begin{Bmatrix} N_a & N_b & N \\ l & J & j_R \end{Bmatrix} \times \begin{Bmatrix} N_a' & N_b' & N' \\ l' & J & j_R' \end{Bmatrix} \begin{Bmatrix} j_R & N_a & J \\ S & J_T & j \end{Bmatrix} \begin{Bmatrix} j_R' & N_a' & J \\ S & J_T & j' \end{Bmatrix} \times \hat{\mathrm{S}}^{J}_{(N_a'N_b')N'l',(N_aN_b)Nl}, \quad \text{(A.5)}$$

which proves Eq. (16).

[1] B. J. Drouin, D. C. Benner, L. R. Brown, M. J. Cich, T. J. Crawford, V. M. Devi, A. Guillaume, J. T. Hodges, E. J. Mlawer, D. J. Robichaud, F. Oyafuso, V. H. Payne, K. Sung, E. H. Wishnow, and S. Yu, "Multispectrum analysis of the oxygen A-band," J. Quant. Spectrosc. Radiat. Transf. **186**, 118–138 (2017).

[2] R. A. Washenfelder, G. C. Toon, J.-F. Blavier, Z. Yang, N. T. Allen, P. O. Wennberg, S. A. Vay, D. M. Matross, and B. C. Daube, "Carbon dioxide column abundances at the Wisconsin Tall Tower site," J. Geophys. Res. **111**, D22305 (2006).

[3] C. E. Miller, D. Crisp, P. L. DeCola, S. C. Olsen, J. T. Randerson, A. M. Michalak, A. Alkhaled, P. Rayner, D. J. Jacob, P. Suntharalingam, D. B. A. Jones, A. S. Denning, M. E. Nicholls, S. C. Doney, S. Pawson, H. Boesch, B. J. Connor, I. Y. Fung, D. O'Brien, R. J. Salawitch, S. P. Sander, B. Sen, P. Tans, G. C. Toon, P. O. Wennberg, S. C. Wofsy, Y. L. Yung, and R. M. Law, "Precision requirements for space-based X_{CO_2} data," J. Geophys. Res. **112**, D10314 (2007).

[4] C. R. Nowlan, C. T. McElroy, and J. R. Drummond, "Measurements of the O_2 *A*- and *B*-bands for determining temperature and pressure profiles from ACE–MAESTRO: Forward model and retrieval algorithm," J. Quant. Spectrosc. Radiat. Transf. **108**, 371–388 (2007).

[5] D. A. Long, D. K. Havey, M. Okumura, H. M. Pickett, C. E. Miller, and J. T. Hodges, "Laboratory measurements and theoretical calculations of O_2 *A* band electric quadrupole transitions," Phys. Rev. A **80**, 042513 (2009).

[6] D. A. Long, D. K. Havey, M. Okumura, C. E. Miller, and J. T. Hodges, "O_2 *A*-band line parameters to support atmospheric remote sensing," J. Quant. Spectrosc. Radiat. Transf. **111**, 2021–2036 (2010).

[7] D. A. Long and J. T. Hodges, "On spectroscopic models of the O_2 *A*-band and their impact upon atmospheric retrievals," J. Geophys. Res. **117**, D12309 (2012).

[8] M. P. Cadeddu, V. H. Payne, S. A. Clough, K. Cady-Pereira, and J. C. Liljegren, "Effect of the Oxygen Line-Parameter Modeling on Temperature and Humidity Retrievals From Ground-Based Microwave Radiometers," IEEE Trans. Geosci. Remote Sens. **45**, 2216–2223 (2007).

[9] D. Cimini, P. W. Rosenkranz, M. Y. Tretyakov, M. A. Koshelev, and F. Romano, "Uncertainty of atmospheric microwave absorption model: impact on ground-based radiometer simulations and retrievals," Atmos. Chem. Phys. **18**, 15231–15259 (2018).

[10] A. Kuze and K. V. Chance, "Analysis of cloud top height and cloud coverage from satellites using the O_2 *A* and *B* bands," J. Geophys. Res. **99**, 14481–14491 (1994).

[11] I. J. Barton and J. C. Scott, "Remote measurement of surface pressure using absorption in the oxygen *A*-band," Appl. Opt. **25**, 3502–3507 (1986).

[12] L. Guanter, L. Alonso, L. Gómez-Chova, M. Meroni, R. Preusker, J. Fischer, and J. Moreno, "Developments for vegetation fluorescence retrieval from spaceborne high-resolution spectrometry in the O_2-*A* and O_2-*B* absorption bands," J. Geophys. Res. **115**, D19303 (2010).

[13] B. R. Judd, *Angular Momentum Theory for Diatomic Molecules* (Academic Press, 1975).

[14] R. R. Gamache, A. Goldman, and L. S. Rothman, "Improved spectral parameters for the three most abundant isotopomers of the oxygen molecule," J. Quant. Spectrosc. Radiat. Transf. **59**, 495–509 (1998).

[15] D. Makarov, I. Koval, M. Koshelev, V. Parshin, and M. Tretyakov, "Collisional parameters of the 118 GHz oxygen line: Temperature dependence," J. Mol. Spectrosc. **252**, 242–243 (2008).

[16] M. Koshelev, I. Vilkov, and M. Tretyakov, "Collisional broadening of oxygen fine structure lines: The impact of temperature," J. Quant. Spectrosc. Radiat. Transf. **169**, 91–95 (2016).

[17] D. S. Makarov, M. Y. Tretyakov, and C. Boulet, "Line mixing in the 60-GHz atmospheric oxygen band: Comparison of the MPM and ECS model," J. Quant. Spectrosc. Radiat. Transf. **124**, 1–10 (2013).

[18] M.A.Koshelev, T.Delahaye, E.A.Serov, I.N.Vilkov, C.Boulet, and M.Yu.Tretyakov, "Accurate modeling of the diagnostic 118-GHz oxygen line for remote sensing of the atmosphere," J. Quant. Spectrosc. Radiat. Transf. **196**, 78–86 (2017).

[19] H. M. Pickett, E. A. Cohen, and D. E. Brinza, "Pressure broadening of oxygen and its implications for cosmic background measurements," Astrophys. J. **248**, L49–L51 (1981).

[20] G. Y. Golubiatnikov, M. A. Koshelev, and A. F. Krupnov, "Reinvestigation of pressure broadening parameters at 60-GHz band and single 118.75 GHz oxygen lines at room temperature," J. Mol. Spectrosc. **222**, 191–197 (2003).

[21] B. J. Drouin, "Temperature dependent pressure induced linewidths of $^{16}O_2$ and $^{18}O^{16}O$ transitions in nitrogen, oxygen and air," J. Quant. Spectrosc. Radiat. Transf. **105**, 450–458 (2007).

[22] D. S. Makarov, M. Y. Tretyakov, and P. W. Rosenkranz, "Revision of the 60-GHz atmospheric oxygen absorption band models for practical use," J. Quant. Spectrosc. Radiat. Transf. **243**, 106798 (2020).

[23] G. C. Corey and F. R. McCourt, "Inelastic differential and integral cross sections for $^{2S+1}\Sigma$ linear molecule - ^{1}S atom scattering: the use of Hund's case (b) representation," J. Phys. Chem. **87**, 2723–2730 (1983).

[24] A. R. Offer, M. C. v. Hemert, and E. F. v. Dishoeck, "Rotationally inelastic and hyperfine resolved cross sections for OH–H_2 collisions. Calculations using a new ab initio potential surface," J. Chem. Phys. **100**, 362–378 (1994).

[25] S. Green, "Rotational excitation in H_2–H_2 collisions: Close-coupling calculations," J. Chem. Phys. **62**, 2271–2277 (1975).

[26] J. M. Brown and A. Carrington, *Rotational Spectroscopy of Diatomic Molecules* (Cambridge University Press, 2003).

[27] W. Gordy and R. L. Cook, *Microwave Molecular Spectra* (John Wiley & Sons, 1984).

[28] H. M. Pickett, "Effects of velocity averaging on the shapes of absorption lines," J. Chem. Phys. **73**, 6090 (1980).

[29] F. Thibault, P. Wcisło, and R. Ciuryło, "A test of H_2-He potential energy surfaces," Eur. Phys. J. D **70** (2016), 10.1140/epjd/e2016-70114-9.

[30] F. Thibault, K. Patkowski, P. Żuchowski, H. Jóźwiak, R. Ciuryło, and P. Wcisło, "Rovibrational line-shape parameters for H_2 in He and new H_2-He potential energy surface," J. Quant. Spectrosc. Radiat. Transf. **202** (2017), 10.1016/j.jqsrt.2017.08.014.

[31] H. Jóźwiak, F. Thibault, N. Stolarczyk, and P. Wcisło, "Ab initio line-shape calculations for the S and O branches of H_2 perturbed by He," J. Quant. Spectrosc. Radiat. Transf. **219**, 313–322 (2018).

[32] M. Słowiński, F. Thibault, Y. Tan, J. Wang, A.-W. Liu, S.-M. Hu, S. Kassi, A. Campargue, M. Konefał, H. Jóźwiak, K. Patkowski, P. Żuchowski, R. Ciuryło, D. Lisak, P. Wcisło, "H_2-He collisions: Ab initio theory meets cavity-enhanced spectra," Phys. Rev. A (2020), 10.1103/PhysRevA.101.052705.

[33] M. Słowiński and et al., "Collisional line-shape effects in accurate He-perturbed H_2 spectra," to be published (2021).

[34] F. Thibault, R. Martínez, D. Bermejo, and P. Wcisło, "Line-shape parameters for the first rotational lines of HD in He," Mol.

Astrophys. (2020), 10.1016/j.molap.2020.100063.
[35]K. Stankiewicz, H. Jóźwiak, M. Gancewski, N. Stolarczyk, F. Thibault, and P. Wcisło, "*Ab initio* calculations of collisional line–shape parameters and generalized spectroscopic cross-sections for rovibrational dipole lines in HD perturbed by He," J. Quant. Spectrosc. Radiat. Transf. **254**, 107194 (2020).
[36]P. Wcisło, F. Thibault, N. Stolarczyk, H. Jóźwiak, M. Słowiński, M. Gancewski, K. Stankiewicz, M. Konefał, S. Kassi, A. Campargue, Y. Tan, J. Wang, K. Patkowski, R. Ciuryło, D. Lisak, R. Kochanov, L. S. Rothman, and I. E. Gordon, "The first comprehensive dataset of beyond-Voigt line-shape parameters from ab initio quantum scattering calculations for the HITRAN database: He-perturbed H_2 case study," J. Quant. Spectrosc. Radiat. Transf. **260**, 107477 (2021).
[37]K. Stankiewicz, N. Stolarczyk, H. Jóźwiak, F. Thibault, and P. Wcisło, "Accurate calculations of beyond-Voigt line-shape parameters from first principles for the He perturbed HD rovibrational lines: a comprehensive dataset in the HITRAN DPL format," J. Quant. Spectrosc. Radiat. Transf. (submitted).
[38]N. Stolarczyk, F. Thibault, H. Cybulski, H. Jóźwiak, G. Kowzan, B. Vispoel, I. Gordon, L. Rothman, R. Gamache, and P. Wcisło, "Evaluation of different parameterizations of temperature dependences of the line-shape parameters based on ab initio calculations: Case study for the HITRAN database," J. Quant. Spectrosc. Radiat. Transf. **240** (2020), https://doi.org/10.1016/j.jqsrt.2019.106676.
[39]H. Jóźwiak, F. Thibault, H. Cybulski, and P. Wcisło, "Ab initio investigation of the CO–N_2 quantum scattering: The collisional perturbation of the pure rotational R(0) line in CO," J. Chem. Phys. **154**, 054314 (2021).
[40]H. Cybulski, C. Henriksen, R. Dawes, X.-G. Wang, N. Bora, G. Avila, T. Carrington, and B. Fernández, "Ab initio study of the CO–N_2 complex: a new highly accurate intermolecular potential energy surface and rovibrational spectrum," Phys. Chem. Chem. Phys. **20**, 12624–12636 (2018).
[41]M. Bartolomei, E. Carmona-Novillo, M. I. Hernández, J. Campos-Martínez, and R. Moszyński, "Global ab Initio Potential Energy Surface for the $O_2(^3\Sigma_g^-)$ + $N_2(^1\Sigma_g^+)$ Interaction. Applications to the Collisional, Spectroscopic, and Thermodynamic Properties of the Complex," J. Phys. Chem. A **118**, 6584–6594 (2014).
[42]H. Klar, "Theory of scattering between two rigid rotors," Z. Physik **228**, 59–67 (1969).
[43]D. Flower, *Molecular collisions in the interstellar medium* (Cambridge University Press, 2007).
[44]In this paper $A_{i,j} \equiv \langle i|A|j\rangle$ are the matrix elements of a given operator A.
[45]T. Orlikowski, "Theoretical studies of rotationally inelastic collisions of molecules in $^3\Sigma$ electronic states: $O_2(X^3\Sigma_g^-)$ + He," Mol. Phys. **56**, 35–46 (1985).
[46]F. Lique, Y. Kalugina, S. Chefdeville, S. Y. T. van de Meerakker, M. Costes, and C. Naulin, "Collisional excitation of O_2 by H_2: the validity of LTE models in interpreting O_2 observations," Astron. Astrophys. **567**, A22 (2014).
[47]F. Lique, "Temperature dependence of the fine-structure resolved rate coefficients for collisions of $O_2(X^3\Sigma_g^-)$ with He," J. Chem. Phys. **132**, 044311 (2010).
[48]F. Lique, A. Spielfiedel, M.-L. Dubernet, and N. Feautrier, "Rotational excitation of sulfur monoxide by collisions with helium at low temperature," J. Chem. Phys. **123**, 134316 (2005).
[49]F. Lique, M.-L. Senent, A. Spielfiedel, and N. Feautrier, "Rotationally inelastic collisions of $SO(X^3\Sigma^-)$ with H_2: Potential energy surface and rate coefficients for excitation by para-H_2 at low temperature," J. Chem. Phys. **126**, 164312 (2007).
[50]Y. Kalugina, J. Kłos, and F. Lique, "Collisional excitation of $CN(X^2\Sigma^+)$ by para- and ortho-H_2: Fine-structure resolved transitions," J. Chem. Phys. **139**, 074301 (2013).
[51]D. L. A. G. Grimminck, F. R. Spiering, L. M. C. Janssen, A. van der Avoird, W. J. van der Zande, and G. C. Groenenboom, "A theoretical and experimental study of pressure broadening of the oxygen A-band by helium," J. Chem. Phys. **140**, 204314 (2014).
[52]P. J. Dagdigian and F. Lique, "Collisional excitation of CH_2 rotational/fine-structure levels by helium," MNRAS **473**, 4824–4831 (2017).
[53]G. C. Corey, M. H. Alexander, and J. Schaefer, "Quantum studies of inelastic collisions of $O_2(X^3\Sigma_g^-)$ with He: Polarization effects and collisional propensity rules," J. Chem. Phys. **85**, 2726–2737 (1986).
[54]G. C. Corey, F. R. McCourt, and W. K. Liu, "Pressure-broadening cross sections of multiplet-Σ molecules: O_2-noble gas mixtures," J. Phys. Chem. A **88**, 2031–2036 (1984).
[55]G. C. Corey, "Rotationally inelastic transitions between the fine-structure levels of the $^3\Sigma_g^-$ electronic ground state of O_2," J. Chem. Phys. **81**, 2678–2683 (1984).
[56]S. Chefdeville, Y. Kalugina, S. Y. T. van de Meerakker, C. Naulin, F. Lique, and M. Costes, "Observation of Partial Wave Resonances in Low-Energy O_2–H_2 Inelastic Collisions," Science **341**, 1094–1096 (2013).
[57]C. K. Bishwakarma, G. van Oevelen, R. Scheidsbach, D. H. Parker, Y. Kalugina, and F. Lique, "Communication: State-to-state inelastic scattering of interstellar O_2 with H_2," J. Chem. Phys. **149**, 121101 (2018).
[58]M. H. Alexander and P. J. Dagdigian, "Propensity rules in rotationally inelastic collisions of diatomic molecules in $^3\Sigma$ electronic states," J. Chem. Phys. **79**, 302–310 (1983).
[59]P. J. Dagdigian, "Interaction of the SH^+ ion with molecular hydrogen: *Ab initio* potential energy surface and scattering calculations," J. Chem. Phys. **150**, 084308 (2019).
[60]M. H. Alexander and P. J. Dagdigian, "Collision-induced transitions between molecular hyperfine levels: Quantum formalism, propensity rules, and experimental study of $CaBr(X^2\Sigma^+)$+Ar," J. Chem. Phys. **83**, 2191 (1985).
[61]S. Green, "Effect of nuclear hyperfine structure on microwave spectral pressure broadening," J. Chem. Phys. **88**, 7331 (1988).
[62]Y. Kalugina and F. Lique, "Hyperfine excitation of CN by para- and ortho-H_2," MNRAS **446**, L21–L25 (2015).
[63]M. Lanza and F. Lique, "Hyperfine excitation of linear molecules by para- and ortho-H_2: Application to the HCl–H_2 system," J. Chem. Phys. **141**, 164321 (2014).
[64]P. J. Dagdigian, "Hyperfine excitation of SH+ in collisions with para- and ortho-H_2," MNRAS **487**, 3427–3431 (2019).
[65]Lique, François, Zanchet, Alexandre, Bulut, Niyazi, Goicoechea, Javier R., and Roncero, Octavio, "Hyperfine excitation of SH^+ by H," A&A **638**, A72 (2020).
[66]R. Zare, A. Schmeltekopf, W. Harrop, and D. Albritton, "A direct approach for the reduction of diatomic spectra to molecular constants for the construction of RKR potentials," J. Mol. Spectrosc. **46**, 37–66 (1973).
[67]L. Monchick and L. W. Hunter, "Diatomic–diatomic molecular collision integrals for pressure broadening and Dicke narrowing: A generalization of Hess's theory," J. Chem. Phys. **85**, 713–718 (1986).
[68]G. Knizia, T. B. Adler, and H.-J. Werner, "Simplified CCSD (T)-F12 methods: Theory and benchmarks," J. Chem. Phys. **130**, 054104 (2009).
[69]K. A. Peterson, T. B. Adler, and H.-J. Werner, "Systematically convergent basis sets for explicitly correlated wavefunctions: The atoms H, He, B-Ne, and Al-Ar," J. Chem. Phys. **128**, 084102 (2008).
[70]D. Feller, K. A. Peterson, and T. D. Crawford, "Sources of error in electronic structure calculations on small chemical systems," J. Chem. Phys. **124**, 054107 (2006).
[71]H. Werner, P. Knowles, G. Knizia, F. Manby, M. Schütz, P. Celani, W. Györffy, D. Kats, T. Korona, R. Lindh, *et al.*, *MOLPRO, version 2019.1, a package of ab initio programs* (University College Cardiff Consultants Ltd.: Cardiff, UK, 2019).
[72]R. Butcher, D. Willetts, and W. Jones, "On the use of a Fabry - Perot etalon for the determination of rotational constants of simple molecules—the pure rotational Raman spectra of oxygen

and nitrogen," Proc. R. Soc. Lond. A **324**, 231–245 (1971).
[73]C. Amiot and J. Verges, "The magnetic dipole $a^1\Delta_g \rightarrow X^3\Sigma_g^-$ transition in the oxygen afterglow," Can. J. Phys. **59**, 1391–1398 (1981).
[74]J. Brown, X.-G. Wang, R. Dawes, and T. Carrington Jr, "Computational study of the rovibrational spectrum of $(OCS)_2$," J. Chem. Phys. **136**, 134306 (2012).
[75]R. Dawes, X. G. Wang, and T. Carrington, "CO dimer: New potential energy surface and rovibrational calculations," J. Phys. Chem. A **117**, 7612–7630 (2013).
[76]X.-G. Wang, T. Carrington Jr, and R. Dawes, "Computational study of the rovibrational spectrum of $(CO_2)_2$," Journal of Molecular Spectroscopy **330**, 179–187 (2016).
[77]E. Castro-Juárez, X.-G. Wang, T. Carrington Jr, E. Quintas-Sánchez, and R. Dawes, "Computational study of the rovibrational spectrum of CO-CO_2," J. Chem. Phys. **151**, 084307 (2019).
[78]J. Brown, X.-G. Wang, T. Carrington Jr, G. S. Grubbs, and R. Dawes, "Computational study of the rovibrational spectrum of CO_2-CS_2," J. Chem. Phys. **140**, 114303 (2014).
[79]R. Dawes, X.-G. Wang, A. W. Jasper, and T. Carrington Jr, "Nitrous oxide dimer: A new potential energy surface and rovibrational spectrum of the nonpolar isomer," J. Chem. Phys. **133**, 134304 (2010).
[80]G. Donoghue, X.-G. Wang, R. Dawes, and T. Carrington, "Computational study of the rovibrational spectra of CO_2-C_2H_2 and CO_2-C_2D_2," Journal of Molecular Spectroscopy **330**, 170–178 (2016).
[81]A. Barclay, A. McKellar, N. Moazzen-Ahmadi, R. Dawes, X.-G. Wang, and T. Carrington, "Infrared spectrum and intermolecular potential energy surface of the CO-O_2 dimer," Phys. Chem. Chem. Phys. **20**, 14431–14440 (2018).
[82]B. Desrousseaux, E. Quintas-Sánchez, R. Dawes, and F. Lique, "Collisional Excitation of CF^+ by H_2: Potential Energy Surface and Rotational Cross Sections," J. Phys. Chem. A **123**, 9637–9643 (2019).
[83]C. T. Bop, F. A. Batista-Romero, A. Faure, E. Quintas-Sánchez, R. Dawes, and F. Lique, "Isomerism Effects in the Collisional Excitation of Cyanoacetylene by Molecular Hydrogen," ACS Earth and Space Chemistry **3**, 1151–1157 (2019).
[84]B. Desrousseaux, E. Quintas-Sánchez, R. Dawes, S. Marinakis, and F. Lique, "Collisional excitation of interstellar PN by H_2: New interaction potential and scattering calculations," J. Chem. Phys. **154**, 034304 (2021).
[85]E. Quintas-Sánchez, R. Dawes, X.-G. Wang, and T. Carrington, "Computational study of the rovibrational spectrum of CO_2-N_2," Physical Chemistry Chemical Physics **22**, 22674–22683 (2020).
[86]E. Quintas-Sánchez and R. Dawes, "AUTOSURF: A Freely Available Program To Construct Potential Energy Surfaces," J. Chem. Inf. Model. **59**, 262–271 (2019).
[87]R. Dawes and E. Quintas-Sánchez, "The Construction of Ab Initio-Based Potential Energy Surfaces," in *Reviews in Computational Chemistry vol. 31* (Wiley, 2018) Chap. 5, pp. 199–264.
[88]M. Majumder, S. A. Ndengue, and R. Dawes, "Automated construction of potential energy surfaces," Mol. Phys. **114**, 1–18 (2016).
[89]A. P. Yutsis, I. B. Levinson, and V. V. Vanagas, *Mathematical Apparatus of the Theory of Angular Momentum* (Israel Program for Scientific Translations, 1962).
[90]H. Jóźwiak, M. Gancewski, K. Stankiewicz, and P. Wcisło, "BIGOS computer code," to be published.
[91]B. R. Johnson, "New numerical methods applied to solving the one-dimensional eigenvalue problem," J. Chem. Phys. **67**, 4086–4093 (1977).
[92]I. E. Gordon, L. S. Rothman, R. J. Hargreaves, R. Hashemi, E. V. Karlovets, F. M. Skinner, E. K. Conway, C. Hill, R. V. Kochanov, V. Boudon, A. Campargue, K. V. Chance, A. Coustenis, B. J. Drouin, J. M. Flaud, R. R. Gamache, J. T. Hodges, D. Jacquemart, E. J. Mlawer, A. V. Nikitin, V. I. Perevalov, M. Rotger, J. Tennyson, G. C. Toon, H. Tran, V. G. Tyuterev, E. M. Adkins, A. Baker, A. Barbe, E. Cané, A. G. Császár, A. Dudaryonokv, O. Egorov, A. J. Fleisher, H. Fleurbaey, A. Foltynowicz, T. Furtenbacher, J. J. Harrison, J. M. Hartmann, V. M. Horneman, X. Huang, T. Karman, J. Karns, S. Kassi, I. Kleiner, V. Kofman, F. Kwabia-Tchana, N. N. Lavrentieva, T. J. Lee, D. A. Long, A. A. Lukashevskaya, O. M. Lyulin, V. Y. Makhnev, W. Matt, S. T. Massie, M. Melosso, S. N. Mikhailenko, D. Mondelain, H. S. P. Müuller, O. V. Naumenko, A. Perrin, O. L. Polyansky, E. Raddaoui, P. L. Raston, Z. D. Reed, M. Rey, C. Richard, R. Tóbiás, I. Sadiek, D. W. Schwenke, E. Starikova, K. Sung, F. Tamassia, S. A. Tashkun, J. V. Auwera, I. A. Vasilenko, A. A. Vigasin, G. L. Villanueva, B. Vispoel, G. Wagner, A. Yachmenev, and S. N. Yurchenko, "The HITRAN2020 molecular spectroscopic database," J. Quant. Spectrosc. Radiat. Transf. (submitted).
[93]P. Wcisło, F. Thibault, M. Zaborowski, S. Wójtewicz, A. Cygan, G. Kowzan, P. Masłowski, J. Komasa, M. Puchalski, K. Pachucki, R. Ciuryło, and D. Lisak, "Accurate deuterium spectroscopy for fundamental studies," J. Quant. Spectrosc. Radiat. Transf. **213**, 41–51 (2018).